

Segmenting the Future

Hsu-kuang Chiu*, Ehsan Adeli*, Juan Carlos Niebles
Stanford University

{hkchiu, eadeli, jniebles}@cs.stanford.edu

Abstract

Predicting the future is an important aspect for decision-making in robotics or autonomous driving systems, which heavily rely upon visual scene understanding. While prior work attempts to predict future video pixels, anticipate activities, or forecast future scene semantic segments from segmentation of the preceding frames, methods that predict future semantic segmentation solely from the previous frame RGB data in a single end-to-end trainable model do not exist. In this paper, we propose a temporal encoder-decoder network architecture that encodes RGB frames from the past and decodes the future semantic segmentation. The network is coupled with a new knowledge distillation training framework specifically for the forecasting task. Our method, only seeing preceding video frames, implicitly models the scene segments while simultaneously accounting for the object dynamics to infer the future scene semantic segments. Our results on Cityscapes outperform the baseline and current state-of-the-art methods. Code is available at https://github.com/eddyhkchiu/segmenting_the_future/.

1. Introduction

Prediction of dynamics in visual scenes is one of the crucial components of intelligent decision-making in robotics and autonomous driving applications [2, 12, 13, 52]. To this end, learning useful representations that enable reasoning about the future has recently been of great attention. Example applications are anticipating activities [43], predicting visual context [49], tracking to the future [23], forecasting human dynamics [5], tracking dynamics in scenes [28, 29], and predicting instance segments [28].

In recent years, semantic and instance segmentation of videos have gained increasing attention [3, 8, 25–27, 51] as the leading means of visual scene understanding to transform the scene into semantic decomposition, such as street, tree, vehicles, pedestrians, and obstacles. These semantic entities provide high-level interpretations of the scene and hence predicting them can be of great interest. Prediction of

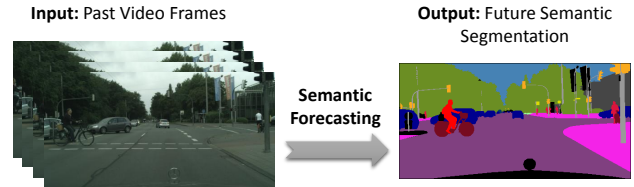


Figure 1. We propose to obtain future semantic segmentation directly from preceding past frames in a single end-to-end trainable model. Our method, hence, requires to implicitly infer the scene semantic segments while also forecasting the future configuration.

pixels in the RGB space is an overly perplexing task, while predicting high-level scene properties is sufficient, can be more useful, and is easier to interpret for decision-making purposes. Towards this direction, previous work predicted future semantic segments given the segmentation of the preceding frames [29, 35], or more sparsely predicted future instance segmentation from previous frames [28]. Whereas, the most useful setting for interpretation of the future is to output future scene semantic segmentation given only the previous RGB frames, even though this is a much harder task compared to the former tasks.

In this paper, we propose a model that predicts the future semantic segmentation in a video from the previous frames, directly from pure RGB data of the frames (see Fig. 1). Inspired by the success of multi-resolution fully convolutional networks (FCN) [3, 8, 26, 27] like U-Net [39] in solving segmentation tasks, we propose an architecture that takes in a temporal sequences of frames and outputs the future semantic segmentation map. Unlike previous work [19, 34, 49] that attempted predicting future RGB video frames from preceding frames, our approach provides future semantic maps, which can enable reasoning about the forthcoming events. Another related previous work [29] adopted a two-stage approach, first using the past RGB sequences to predict the future RGB frame, and then generating the future segmentation on top of that. The performance of this approach is not satisfactory due to the difficulty of predicting future pixel values. On the contrary, one of our key observation is that future frame pixel values are *not* necessary for generating future semantic segmentation. We propose a single stage end-to-end trainable model

*equal contribution lead author

that does not require predicting the future RGB frame as an intermediate step. In this setting, our method learns to implicitly model the scene segments, and simultaneously account for the intrinsic dynamics of semantic maps of different object categories to predict future segmentation. In particular, this is a challenging task as objects in the semantic maps can significantly deform over the video frames (due to changes in camera viewpoint, illumination, or orientation). To alleviate these challenges, our architecture encodes the sequence of input frames in a multi-resolution manner into a collective latent representation, and then decodes this representation gradually to the future semantic map. We also propose a new knowledge distillation [15] training framework to further refine the future semantic map. During the training stage, we utilize a fixed pre-trained single frame segmentation model and use it as a ‘teacher network.’ Taking the future frame as the input, it predicts the future segmentation. The predicted output from the teacher network provides additional information to guide the training of our main forecasting model, denoted by ‘student network.’ This introduces one more training loss component, called distillation loss, which measures the difference between the outputs of the teacher and student networks. During inference, the teacher network is not used and the student network itself forecasts the future semantic segmentation by taking only the past RGB sequence as the input.

To evaluate the performance of our method, we use the Cityscapes dataset [6] for predicting future video semantic segmentation under several different scenarios, and compare our results with previously published methods. We predict the future semantic maps of three different time-steps ahead (*i.e.*, short-term, mid-term, and long-term) from the preceding RGB frames. Our method outperforms the previous state-of-the-arts although solving a much harder problem of predicting all semantic segments by only using past raw image sequences as input.

In summary, our contributions are two-fold. First, we propose a single-stage end-to-end trainable model for the challenging task of predicting future semantic segmentation based on only the preceding RGB frames. Second, we propose a new knowledge distillation training framework. We introduce an additional distillation loss using a teacher network during training. We show that although this is a challenging task, our method can uncover the relations between the previous and future frames while taking the motion into account. Our proposed method does not require extremely costly semantic segmentation maps for the previous frames, in contrast, it predicts the future semantic map directly from preceding RGB frames.

2. Related Work

Semantic and Instance Segmentation Semantic segmentation problems are often modeled by fully convolutional

architectures (FCN) with multiple scales, such as [8, 26, 27, 34, 39], or sometimes by larger receptive fields ([3, 30, 53]). On the other hand, instance segmentation often maintains an strategy to generate instance-proposal regions [7, 38] as part of the segmentation pipeline. Some of the early methods for this task integrate object detection and segmentation in a sequential manner [7, 48], and more recently in a joint multi-task end-to-end framework [24].

Other works have explored the utilization of temporal information and consistency across frames. Some of them are based on 3D data structures and operations [50] or CRF models [21, 32], and some others leveraged optical flow [4, 40]. More recently, a number of methods utilize predictive feature learning techniques to enhance video segmentation result. For instance, Jin *et al.* [17] built a predictive model to learn features from the preceding input frames. All the above previous works aim at segmenting the last seen frame. They do not evaluate their predictive power of the learned features for segmenting the future.

Video Forecasting There has been a growing interest in predicting and forecasting visual data. Such forecasting task was defined as extrapolating video pixels to create realistic future frames [10, 34, 44–46, 49]. Although these methods have some success in predicting the future in a pixel-level, modeling raw RGB pixel values is rather cumbersome in comparison with predicting the future more high-level properties of the video. These high-level properties can not only be sufficient for analysis in many applications but also be more beneficial due to higher level of semantic abstraction. For instance, many recent works focused on anticipating activities and events in video scenes [16, 20, 22, 43, 49] or explicitly forecasting human trajectories in future frames [1, 5, 23].

One of the best procedures for understanding and parsing the scenes is scene semantic segmentation [50]. Recently, a few works proposed techniques for predicting semantic segmentation in videos. For instance, Luc *et al.* [29] defined future semantic segmentation prediction through various configurations. They predicted future scene segmentation either from segmentation of the preceding frames or from the combination of segmentation and RGB data of the previous frames. They also presented a two-stage approach that first predicts the future frame pixel values, and then generates segmentation maps on top of the predicted future frame. Similarly, Jin *et al.* [18] and Navabi *et al.* [35] predicted the future segmentation from previous frame segmentation maps. Jin *et al.* [18] developed a method based on flow anticipation using convolutional neural networks and Nabavi *et al.* [35] developed a convolutional LSTM (ConvLSTM) model. In another work, Luc *et al.* [28] developed a predictive model with fixed-sized features of the Mask R-CNN for future instance segmentation. Their work can only predict the future movement for limited types of objects, but

Table 1. Task setting comparisons with prior work. Our work proposes a single-stage end-to-end trainable model on forecasting future semantic segmentation (Seg) given only past RGB sequence.

Model	Input	Output
X2X [29]	RGB	RGB
S2S [29]	Seg	Seg
XS2X [29]	RGB + Seg	RGB
XS2S [29]	RGB + Seg	Seg
XS2XS [29]	RGB + Seg	RGB + Seg
ConvLSTM [35]	Seg	Seg
Ours	RGB	Seg

not for other critical classes of importance for autonomous driving applications, such as roads and buildings. In summary, Luc *et al.* [29] and Nabavi *et al.* [35] are the closest related works to ours, since they also target on forecasting future semantic segmentation. However, their models mainly rely on past semantic segmentation sequence as the input, or a two-stage approach via forecasting future RGB frame as an intermediate step, as shown in Table 1. In contrast to those previous works, we introduce a single-stage end-to-end trainable model for the problem of predicting the future semantic segmentation solely based on the preceding RGB frames, which can be better suited for intelligent systems requiring to make instant decisions for the near future.

Knowledge Distillation Knowledge distillation [15] was originally proposed to compress the knowledge from an ensemble of models into a single model during the training. Further works [31, 37, 42] extend this idea to distill knowledge from different data modalities, such as optical flow and depth information for action recognition and video classification tasks. Different from all previous works, we propose a teacher network that takes the input from the same modality, the RGB frame, but in a different temporal range.

3. Method

Our goal is to build a model to forecast the future semantic segmentation given the past RGB sequence as the inputs. To this end, we solve the semantic segmentation and forecasting problems jointly in a single end-to-end trainable model. Our proposed architecture is designed as the integration of the two networks, the **student network** and the **teacher network**. The student network is designed to perform our main forecasting task. During training, the teacher network uses the future RGB frame to provide additional guidance to help the student network reach the optimization target. At inference, the teacher network is not used, and the student network itself completes the forecasting, without knowing anything about the future RGB frame and the future segmentation (See Fig. 2).

The student network, as shown in the upper half of Fig. 2, has the three main components: encoder, forecasting module, and decoder. The **encoder** module generates feature maps in multiple resolutions from each input frame. Sup-

pose the video is observed up to time t . The frame at time t and three frames before that form the input to the network. Formally, the inputs are X_{t-3d} , X_{t-2d} , X_{t-d} , and X_t , where d denotes the displacement between each pair of the preceding frames. Then, the **forecasting module** uses the feature maps (the lowest level maps from each past frame pathway) to learn a latent-space representation by consolidating temporal dynamics across them. This module uses a temporal 3D convolution structure and acts as a predictive feature learning module integrating feature maps from the preceding frames. Finally, the **decoder** combines the spatial feature maps (through skip connections to the encoder) and the temporal features (output of the Conv3D module) to generate the final semantic segmentation in the future at time $t+d'$ (d' denotes the time delay in the future, for which the semantic segmentation is sought). Hence, the ground-truth future segmentation is referred to by $S_{t+d'}$, and the prediction by $\hat{S}_{t+d'}$. The choice of d' defines how far in the future we plan to segment. We experiment on three different settings of the combinations of d and d' for short-term, mid-term, and long-term semantic segmentation forecasting.

The lower half of Fig. 2 shows how the teacher network is used to generate the additional loss term to help train the student network. Unlike X2X [29] that used the future RGB frame as an intermediate training target, our model uses the future frame in a new knowledge distillation approach during the training time. The teacher network can be any fixed pre-trained single frame semantic segmentation network. It uses the future frame $X_{t+d'}$ as the input to predict the future semantic segmentation. The difference between the pre-softmax output features from the teacher network and the one from the student network is used as the additional training loss. During inference, the teacher network and any information from the future are not used. The output of the student network is used as the output of our model.

3.1. Student Network

This network is the main component of our model that performs the forecasting task during both training and inference time, as shown in the upper half of Fig. 2. The student network contains three main components: past encoder, forecasting module, and future decoder to perform our main forecasting task. The supplement outlines detailed architecture of the student network.

Past Encoder Our forecasting architecture is inspired by the encoder-decoder FCN models [3, 8, 26, 27] commonly used for segmentation tasks, such as U-Net [39]. However, in contrast to nearly all previous semantic segmentation methods, our encoder module contains parallel pathways, one for each input preceding frame. Each pathway contains a series of fully convolutional neural networks, non-linearity layers, and max-pooling layers, to generate the feature maps in multiple resolutions.

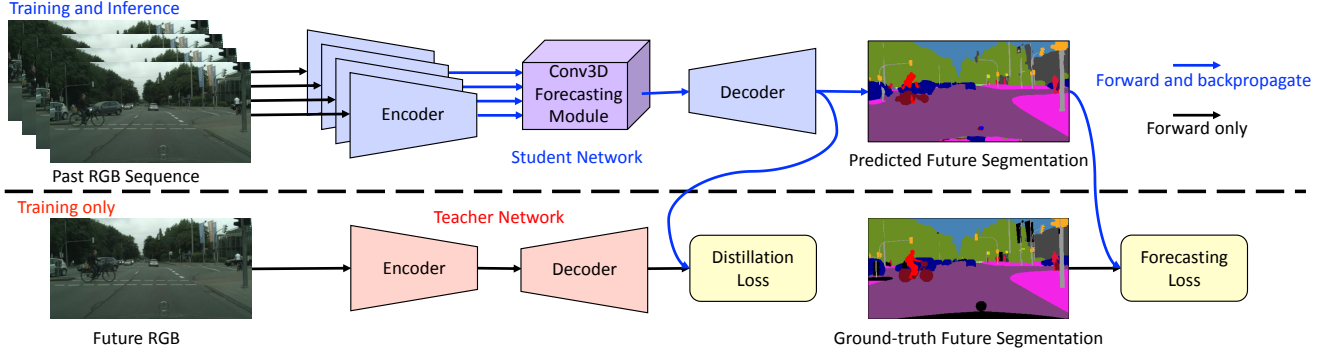


Figure 2. Architecture overview: our student network contains encoder, forecasting module, and decoder to forecast future semantic segmentation. During training, we have another fixed pre-trained teacher network, which takes the future RGB frame as input and predicts the future semantic segmentation. The overall training loss is the weighted sum of the cross-entropy forecasting loss and the mean-squared error distillation loss. During inference, the teacher network is not used and the student network performs the forecasting task by itself.

The encoder can be designed using the common image classification models, such as VGG [41] or ResNet [14], where the feature maps in different resolutions can be extracted right before each max-pooling layer. In our proposed method, we choose VGG19 with batch normalization as our encoder backbone. For each input frame X_i , we first generate the feature map in the highest resolution by feeding it into two convolution modules, each of which contains a 3×3 2D convolutional layer (Conv2D), a batch normalization (BN) layer, and a rectified linear unit (ReLU). Then, the first feature map is fed into a max-pooling layer and another set of two convolution modules to generate the next feature map in a lower resolution. Similar operations are applied to generate all feature maps in different resolutions. Please see the supplementary material for more details.

Forecasting Module In contrast to most of the previous semantic segmentation models that only use two encoder and decoder modules, our model introduces a forecasting module to focus on learning predictive features and temporal dynamics representations. For this purpose, we choose a 3D convolution network to combine the encoded feature maps in the lowest resolution of each encoder pathway (from each past time-step).

This is a simple design choice, but proves to be most accurate one compared to LSTM [11] or ConvLSTM [47] in our experiments. In addition to this 3D convolution pathway between the encoder and the decoder, skip connections provide another set of interactions between them.

Future Segmentation Decoder The decoder takes the encoded feature maps at each resolution and the temporal dynamics representation as inputs and generates the future semantic segmentation, \hat{S}_{t+d} . Different decoder structures are often used in previous semantic segmentation models including FCN [27] or Feature Pyramid Network [26] (FPN). As an example, the previous state-of-the-art semantic segmentation forecasting model, ConvLSTM [35], reused the

decoder structure of FPN [26] with 1×1 convolution, up-sampling, and element-wise addition to obtain the segmentation at the original resolution.

We build our decoder symmetric to the encoder module sequence, as illustrated in the supplementary material (similar to U-Net [39]). This choice gives us more computation capacity than the FPN decoder. Furthermore, the feature maps from different resolutions of the encoder can be directly concatenated with their counterparts in the decoder pathway. Such skip connections have shown to be very useful for maintaining fine boundary information as the features maps are gradually expanded in resolution [36, 39]. As a result of this symmetric structure, the lower level feature representation can be fed to the transpose convolution layer, which contains trainable parameters and upsamples the lower resolution feature to a higher resolution. Then, it is concatenated with the encoder feature maps of the corresponding resolution from the latest past time-step followed by a sequence of 2D convolution modules. Similar to the encoder, these sequence of modules are applied multiple times until we reach the original resolution.

To construct the future segmentation from the decoder, the final convolution layer of the decoder generates a pre-softmax output tensor O with shape $H \times W \times C$, where H and W are the height and the width of the frames, and C is the number of semantic categories. This output tensor O is then applied with a soft-max function to generate the predicted probability distribution tensor P of the same shape $H \times W \times C$:

$$P(h, w, c) = \frac{\exp(O(h, w, c))}{\sum_{i=1}^C \exp(O(h, w, i))}, \quad (1)$$

where h, w are the coordinates of a pixel, and c is the index of each semantic class. O is the pre-softmax output tensor of the student network. $P(h, w, c)$ represents the predicted probability that the pixel at (h, w) belongs to semantic category c . For each pixel $x = (h, w) \in \{H \times W\}$ and each

semantic class c , we define the predicted probability function $p_c(x)$:

$$p_c(x) = P(h, w, c), \quad (2)$$

where $x = (h, w)$ represents the index of a pixel in the frame. To generate the final forecasting output, we choose the class with the highest probability as our predicted semantic segmentation result $\hat{S}_{t+d'}$ for that pixel:

$$\hat{S}_{t+d'}(x) = \underset{c}{\operatorname{argmax}} p_c(x), \quad (3)$$

where $\hat{S}_{t+d'}(x)$ is the predicted future semantic class for the pixel $x = (h, w)$ at time $t + d'$.

3.2. Training Loss and Teacher Network

Another important component of our model is the teacher network, as shown in the lower half of the Fig 2. During the training, our loss L is defined as the combination of the forecasting loss L_f and the distillation loss L_d using weighted sum $L = L_f + \lambda L_d$, where λ is a hyperparameter. The forecasting loss L_f measures the difference between the predicted output of the model $\hat{S}_{t+d'}$ and the ground-truth semantic segmentation $S_{t+d'}$. We use the cross-entropy function to define this classification loss:

$$L_f = -\frac{1}{HW} \sum_{x \in \{H \times W\}} \log(p_{g(x)}(x)), \quad (4)$$

where $g(x) \in \{1, \dots, C\}$ defines the ground-truth label for pixel x . The second loss term L_d is used to measure the difference between the outputs from the student network and the teacher network. As mentioned earlier, the teacher network is a fixed pre-trained single frame segmentation model. We let the teacher network have the same encoder and decoder architecture as the student network, but without sharing the trainable parameters. The teacher network takes the future RGB frame $X_{t+d'}$ as input and generates its own predicted future semantic segmentation $\hat{S}_{t+d'}^{te}$. Instead of directly comparing the predicted semantic segmentation, we define the distillation loss L_d using the mean squared error between the pre-softmax output tensors from the student network and the teacher network:

$$L_d = \frac{1}{HWC} \sum_{h=1}^H \sum_{w=1}^W \sum_{c=1}^C (O(h, w, c) - O_{te}(h, w, c))^2, \quad (5)$$

where O is the pre-softmax output tensor from the student network, and O_{te} is the one from the teacher network. With this distillation loss L_d , the single frame semantic segmentation teacher network provides additional regression guidance to help the student network learn to forecast future semantic segmentation. During training, we minimize the overall loss L . During inference, the predicted output of the student network $\hat{S}_{t+d'}$ is the final output of our model.

Note that we split the dataset into the training set and the validation set. The future RGB frame information of the training set is only used in the training stage. The future

RGB frame information of the validation set is never used in any training step or any validation step. Therefore, during inference, our model only takes the past RGB sequences as input, and directly forecasts the future semantic segmentation as the output, without using any extra information.

4. Experimental Results

We evaluate our algorithm on a challenging and widely used dataset. We compare the results with several baseline and state-of-the-art algorithms.

Dataset: Similar to several previous works [28, 29, 35], we use the Cityscapes dataset. It is a large-scale dataset containing pixel-wise annotations for some frames. In the training, validation, and testing sets, the dataset provides 2975, 500, and 1525 annotated frames with 19 semantic classes. Another set of 20,000 coarsely annotated frames are also provided. In each of the video clips of length 30 (frames are indexed 0 to 29), the dataset provides fine annotations for the 19th frame. In total there are 180,000 frames of resolution of 1024×2048 pixels. Following the same setting of previous work [29, 35], we only use the finely annotated frames for training, and downsample the frames to resolution of 256×512 . We train our model using the Adam optimizer with initial learning rate 0.001, and batch size 8. We set the hyperparameter combining the loss terms λ to be 100, so that the two loss terms have similar numerical scale in the beginning of training. Besides, we initialize our teacher network by training a single frame segmentation model using the same dataset. We initialize the encoder of the student network with ImageNet [9] pre-trained weights.

Settings: In our problem setting, the input is the past RGB frame sequence and we aim to forecast the future semantic segmentation. Following the forecasting settings in the related previous works [29, 35], we design three experimental settings on different time-ranges: short-term, mid-term, and long-term. For all settings, we always define the 19th frame in the Cityscapes sequences, denoted by S_{19} , as the target frame for forecasting, since the ground-truth semantic labels for this frame is available. The input RGB frames are selected from different timesteps in the past, denoted by X_i , depending on the forecasting time-range setting. For short-term forecasting, the input RGB frames are $X_{15}, X_{16}, X_{17}, X_{18}$; for mid-term forecasting $X_7, X_{10}, X_{13}, X_{16}$; and for long-term forecasting they are X_1, X_4, X_7, X_{10} , while the output for all is \hat{S}_{19} .

Evaluation Metrics: Following previous practice, we use the mean Intersection Over Union (mIOU) as the performance metric for segmentation evaluation. We further report pixel-level accuracy (pAcc) and mean per-class accuracy (mAcc). Specifically, mIOU is the pixel IOU averaged across all classes; pAcc defines the percentage of correctly classified pixels; and mAcc is the average class accuracies.

Table 2. Evaluation of our method in terms of mIOU, pixel-level accuracy (pAcc), and mean category accuracy (mAcc) in comparison with baseline and relevant methods on forecasting future semantic segmentation using past RGB sequence as the inputs. In each column, the best obtained results are typeset in boldface and the second best are underlined. *X2X is not the main focus of [29], and only the mid-term mIOU result is reported in this setting. **Our implementation of [35], adapted to our input/output setting.

Model	Short-term			Mid-term			Long-term		
	mIOU	pAcc	mAcc	mIOU	pAcc	mAcc	mIOU	pAcc	mAcc
Zero-motion	<u>58.91</u>	<u>91.96</u>	<u>69.68</u>	48.15	<u>87.89</u>	<u>59.67</u>	<u>36.21</u>	<u>81.77</u>	<u>47.07</u>
Two-stage	49.17	90.22	61.68	26.53	74.60	36.19	9.64	44.86	14.49
X2X* [29]	-	-	-	23.00	-	-	-	-	-
ConvLSTM** [35]	45.08	89.28	54.15	36.81	85.79	45.57	27.36	80.44	24.63
Ours	65.08	93.83	74.36	56.98	91.38	67.67	40.81	86.03	50.13

4.1. Baseline Methods

We use the ConvLSTM [35] model as our main comparison baseline. ConvLSTM [35] achieves the state-of-the-art performance on a slightly different segmentation forecasting task. In their task setting, the inputs are the past segmentation sequences. Although our experiment setting is different, which uses the past raw image frames as the inputs, ConvLSTM [35] can still be a strong baseline model. The architecture of ConvLSTM is based on the novel bidirectional ConvLSTM temporal module. Furthermore, it uses the asymmetric Resnet101-FPN encoder-decoder backbone structure. ConvLSTM [35] model outperforms the previous state-of-the-art S2S [29] in the same task setting.

Additionally, Luc *et al.* [29] has an X2X architecture, which is also used as our other baseline. Luc *et al.* [29] focused on the same problem setting as the one of ConvLSTM [35]. However, they also presented an X2X [29] architecture that uses the past RGB sequences to forecast the future RGB frame and then generate the future segmentation. We argue that it is not necessary to generate the future RGB frame as an intermediate step. Since [29] only presents the result in the mid-term time-range setting, we further implement a two-stage model based on the same idea.

Another important baseline is denoted by ‘zero-motion’. This is the case that no motion is anticipated in the video and the future frame semantic segmentation is identical to that of the last observed frame. Although this is a very naïve baseline, it poses as a very challenging one [5, 33], especially for short-term forecasting. To calculate this metric, we first train a single frame semantic segmentation model. Then, we apply it to the last input image frame and use the generated segmentation map as the predicted future result.

4.2. Quantitative Results

Table 2 shows the results of our method on the Cityscapes dataset, compared with the previous state-of-the-art semantic segmentation forecasting model ConvLSTM [35], the two-stage model X2X [29], and other baseline methods. Note that the previous work ConvLSTM [35] focused on predicting future segmentation directly from past semantic segmentation as the inputs. Therefore, we re-implemented their model, but training and testing using

past RGB sequences as the inputs. As can be seen in Table 2, our model outperforms ConvLSTM [35] by a large margin in all the three time-ranges. That supports our design choice of using the symmetric encoder-decoder backbone and the Conv3D temporal module in our forecasting model. We can also see the significant performance difference between the two-stage models, including X2X [29], and our proposed single-stage model. The performance difference supports our argument that forecasting future RGB frame is not necessary for forecasting future semantic segmentation. Besides, our method outperforms the the zero-motion baseline for all three time-ranges. Interestingly, ConvLSTM [35], X2X [29], and some of the other compared methods perform worse than the zero-motion naïve baseline.

Ablation Table 3 shows the ablation analysis results on our model to examine where the performance improvements derive from. The main architecture difference between our model and the previous works are the symmetric encoder-decoder backbone, the Conv3D temporal forecasting module, and the distillation training.

First, to evaluate whether our symmetric encoder-decoder backbone design is the key for the performance boost, we create another model by replacing our backbone architecture with the asymmetric one as in ConvLSTM [35], which simply uses the decoder of FPN as their backbone decoder. The results of this asymmetric backbone model are shown in the first row of table 3. We can see that all the evaluation metrics are worse than our proposed model significantly. As mentioned earlier in the Method Section, our proposed symmetric backbone decoder is designed with more computational capacity compared to FPN decoder. That design decision is due to the fact that in our problem setting, the inputs and outputs representing two different types of information, the image and the segmentation. They are potentially far away from each other in the latent representation space. Therefore, more computation capacity is required, compared with previous works [29, 29] whose inputs and outputs are all segmentation data.

Next we analyze the impact of the temporal structures. We implement two other models by replacing our Conv3D temporal module with LSTM [11] and the multi-resolution Conv3D. The results are reported in the second and the

Table 3. Ablation results: evaluation of our method in terms of mIOU, pixel-level accuracy (pAcc), and mean category accuracy (mAcc) in comparison with variations of our method on forecasting future semantic segmentation using past RGB sequence as the inputs. In each column, the best obtained results are typeset in boldface and the second best are underlined.

Model	Short-term			Mid-term			Long-term		
	mIOU	pAcc	mAcc	mIOU	pAcc	mAcc	mIOU	pAcc	mAcc
Ours w/o symmetric backbone	47.80	89.65	57.31	39.37	87.03	47.72	28.22	81.51	35.95
Ours w/o Conv3D temporal module	48.22	90.26	58.39	39.57	86.93	49.18	26.61	81.46	33.19
Ours w/ Multi-Res Conv3D	59.24	93.24	69.44	49.33	90.38	59.39	36.96	85.42	45.98
Ours w/o distillation loss	<u>63.60</u>	<u>93.76</u>	<u>73.01</u>	<u>55.97</u>	<u>91.17</u>	<u>66.59</u>	<u>40.32</u>	<u>85.84</u>	<u>49.69</u>
Ours	65.08	93.83	74.36	56.98	91.38	67.67	40.81	86.03	50.13

third rows of Table 3. As suggested by the results, the LSTM module has significantly negative impact. The multi-resolution Conv3D temporal module contains total five Conv3D layers, each of which takes the past feature maps from different resolution and generates the dynamic information for the decoder. Intuitively, we expect that this approach performs even better than our model. But empirically, we observe performance decrease, as shown in the third row of the table. One possible reason is that the larger number of trainable parameters makes the model easily prone to over-fitting. Furthermore, this approach requires more memory, which forces the model to operate on a smaller batch size. Therefore, the regularization effect from the batch normalization layer becomes less effective.

Finally, we analyze the impact of the student-teacher architecture and the distillation training loss. Without the teacher network and the distillation training loss, results of our student-only model are shown in the fourth row of Table 3. Note that our student-only model already outperforms other previous works shown in Table 2. Our final proposed model uses the decoder output of the teacher network to define the distillation loss as in Equation (5). We can see that the mIOU scores further improve by 0.5% to 1.5% mIOU scores for all the three time-range settings, compared with our student-only model.

4.3. Qualitative Results

Mid-term forecasting: We start this section with the mid-term forecasting results as this is the most widely used setting in the previous work for evaluation. Fig. 3(b) shows the qualitative results, which uses the past RGB sequence $X_7, X_{10}, X_{13}, X_{16}$ to forecast the future semantic segmentation at time-step 19, denoted as S_{19} . In this figure, each row is a separate sample sequence, and the left most column is the past RGB input sequence, followed by the ground-truth future semantic segmentation in the second column, our predicted future semantic segmentation in the third column, ConvLSTM [35] results in the fourth column, and the two-stage method results in the last column.

The first row shows examples where the camera is moving forward. Our model accurately captures the relative motion dynamic between the camera and all the objects in the scene. Our prediction results show that the right-side street-parking car segmentation moves toward right further, sim-

ilar to the ground-truth. The example in the second row shows that our model can capture and predict the future based on different motion patterns. In this sample, the camera is relatively static. However, the pedestrians, bike, and cars are moving toward different directions in the scene. Our model is able to distinguish each object and identify their moving directions. Specifically, a biker and a car are moving toward each other, with different distances to the camera. Our model is able to predict these two segments will intersect in the future frame, but was unable to really figure out which one should be in the foreground due to the lack of distance information. This problem can be an interesting future research work, potentially solvable by including additional depth information if provided.

Short-term forecasting: For the short-term forecasting experiment setting, we can see that our model precisely predicts both the directions and the magnitude of the movements for the cars, as shown in Fig. 3(a). In the first row, the car is moving toward right, and the predicted car position in the future frame is the same as that in the ground-truth. In the second example, the left parked car is moving out of the frame due to the camera motion. Again, our model captures the exact relative motion dynamic information and precisely forecasts the same shape, size, and location of the area occupied by the same parked car in the future frame. Another interesting issue is that the ground-truth annotation of the second example actually misses the circle direction sign (yellow color in the segmentation map) while our model is capable to detect that direction sign segment and place it in the right position in the future frame.

Long-term forecasting: In addition, Fig. 3(c) shows the long-term forecasting results. Our model uses the past RGB image sequence X_1, X_4, X_7, X_{10} as the inputs, and generate the future semantic segmentation S_{19} , which is 9 steps in the future from the last input frame. Such setting is more challenging than mid-term and short-term forecasting; however, our model can still accurately predict the moving directions of the parked cars (specially in the first example) and the pedestrians in the second example. In comparison with the ground-truth, although our results correctly predict the moving directions, we can notice that the magnitude of the movements seem to be smaller than the ground-truth. This may be due to changes in the speeds of the objects in the frames that are not observed by our model.

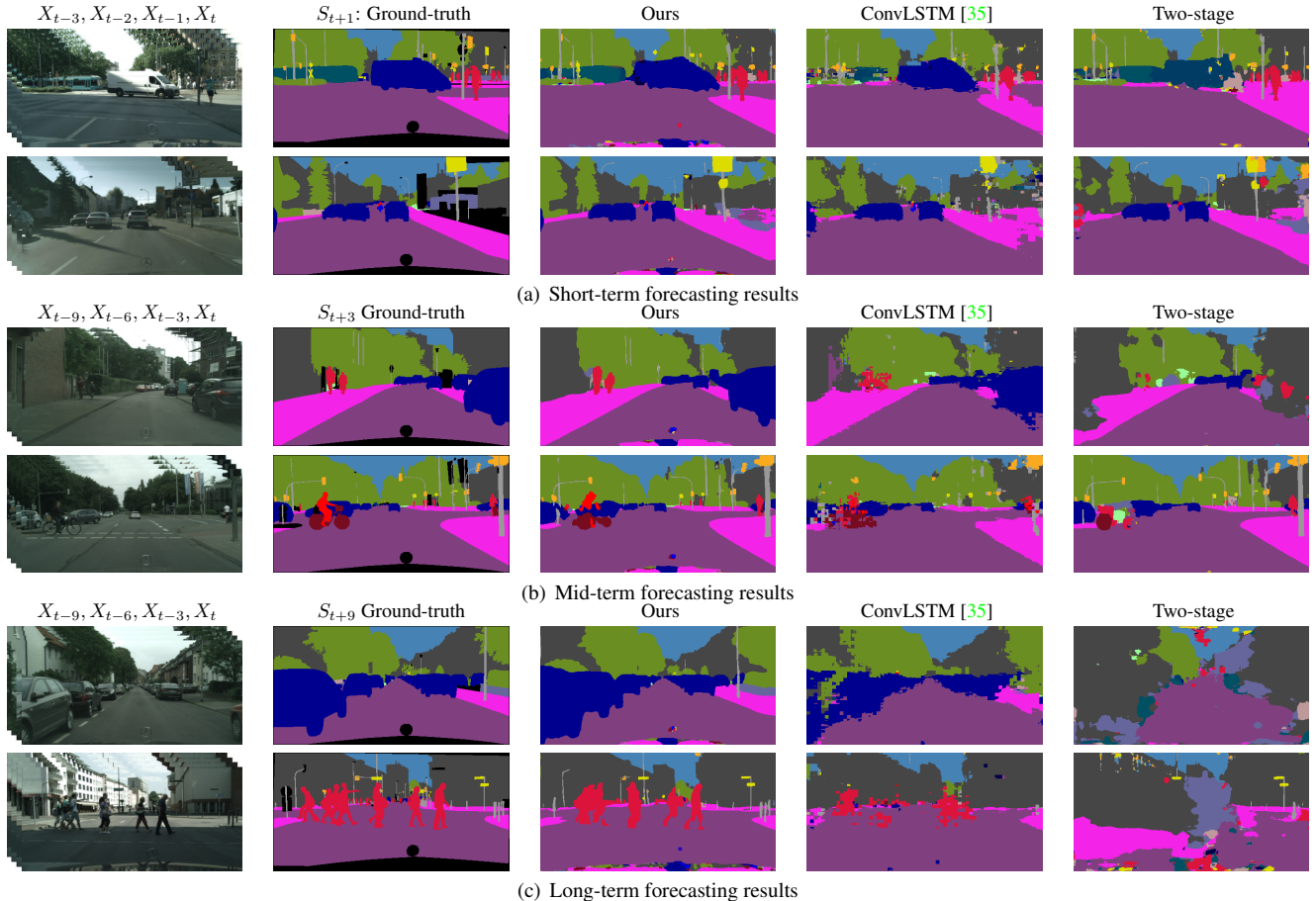


Figure 3. Qualitative results. \hat{S} denotes the prediction segmentation and S the ground-truth. Each row corresponds to a different video. In all three cases, the semantic segmentation prediction is done using the preceding four frames with different lengths of time horizon in the future, *i.e.*, $d' = 1, 3,$ and 9 for short, mid, and long-term forecasting, respectively. See supplementary material for more results.

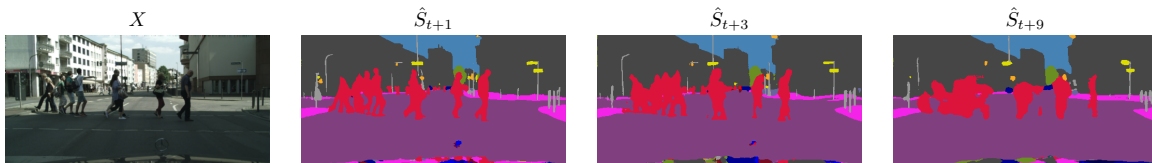


Figure 4. Forecasting results of three different time-range settings, based on the same data sample. Here, X is the last frame of the input RGB sequence. $\hat{S}_{t+1}, \hat{S}_{t+3}, \hat{S}_{t+9}$ denotes the predicted future segmentation of short-, mid-, and long-term settings, all corresponding to the same X .

Time-horizon comparison: Fig. 4 shows the forecasting results for our three time horizons. For all these settings, we use the same frame, namely X_{16} , as the last frame of the input sequence. We can see that the short-term forecasting result provides the best visual quality. From the mid-term result, we can still see that the segmentation boundary of the pedestrians are still reasonable. But for the long-term result, their shapes start to deform away from regular pedestrian appearance. However, we still can see that different groups of the pedestrians moving toward their destination in the correct directions with reasonable amount of moving distances from our three prediction results.

5. Conclusion

In this paper, we proposed a single-stage end-to-end trainable model for the challenging problem statement of predicting future frame semantic segmentation having only observed the preceding frames RGB data. This is a practical setting for autonomous systems to directly reason about the near future based on current video data without the need to acquire any other forms of meta-data. Our proposed model for solving this task included several encoding pathways to encode the past, a temporal 3D convolution structure for capturing the scene dynamics and predictive feature learning, and finally a decoder to gradually reconstruct

the future semantic segmentation. We further proposed a teacher network coupled with a distillation loss for training the network to improve the overall forecasting performance. The results on the popular Cityscapes dataset indicates that our method can predict future segmentation and outperform several baseline and state-of-the-art methods.

Acknowledgements. This work was partially funded by Oppo and Panasonic. The authors would like to thank Jingwei Ji and Damian Mrowca for their feedback on the paper.

References

- [1] A. Alahi, V. Ramanathan, and L. Fei-Fei. Socially-aware large-scale crowd forecasting. In *Proceedings of the IEEE Conference on Computer Vision and Pattern Recognition*, pages 2203–2210, 2014. 2
- [2] W. Byeon, Q. Wang, R. K. Srivastava, and P. Koumoutsakos. Contextvp: Fully context-aware video prediction. In *European Conference on Computer Vision (ECCV), Munich, Germany*, 2018. 1
- [3] L.-C. Chen, G. Papandreou, I. Kokkinos, K. Murphy, and A. L. Yuille. Deeplab: Semantic image segmentation with deep convolutional nets, atrous convolution, and fully connected crfs. *IEEE transactions on pattern analysis and machine intelligence*, 40(4):834–848, 2018. 1, 2, 3
- [4] J. Cheng, Y.-H. Tsai, S. Wang, and M.-H. Yang. Segflow: Joint learning for video object segmentation and optical flow. In *ICCV*, pages 686–695. IEEE, 2017. 2
- [5] H.-k. Chiu, E. Adeli, B. Wang, D.-A. Huang, and J. C. Niebles. Action-agnostic human pose forecasting. In *WACV*, 2019. 1, 2, 6
- [6] M. Cordts, M. Omran, S. Ramos, T. Rehfeld, M. Enzweiler, R. Benenson, U. Franke, S. Roth, and B. Schiele. The cityscapes dataset for semantic urban scene understanding. In *Proceedings of the IEEE conference on computer vision and pattern recognition*, pages 3213–3223, 2016. 2
- [7] J. Dai, K. He, Y. Li, S. Ren, and J. Sun. Instance-sensitive fully convolutional networks. In *ECCV*, pages 534–549. Springer, 2016. 2
- [8] J. Dai, Y. Li, K. He, and J. Sun. R-fcn: Object detection via region-based fully convolutional networks. In *Advances in neural information processing systems*, pages 379–387, 2016. 1, 2, 3
- [9] J. Deng, W. Dong, R. Socher, L.-J. Li, K. Li, and L. Fei-Fei. ImageNet: A Large-Scale Hierarchical Image Database. In *CVPR09*, 2009. 5
- [10] C. Finn, I. Goodfellow, and S. Levine. Unsupervised learning for physical interaction through video prediction. In *Advances in neural information processing systems*, pages 64–72, 2016. 2
- [11] F. A. Gers, J. Schmidhuber, and F. Cummins. Learning to forget: Continual prediction with lstm. 1999. 4, 6
- [12] L.-Y. Gui, Y.-X. Wang, D. Ramanan, and J. M. Moura. Few-shot human motion prediction via meta-learning. In *European Conference on Computer Vision (ECCV), Munich, Germany*, 2018. 1
- [13] A. Gupta, J. Johnson, L. Fei-Fei, S. Savarese, and A. Alahi. Social gan: Socially acceptable trajectories with generative adversarial networks. In *IEEE Conference on Computer Vision and Pattern Recognition (CVPR)*, number CONF, 2018. 1
- [14] K. He, X. Zhang, S. Ren, and J. Sun. Deep residual learning for image recognition. In *Proceedings of the IEEE conference on computer vision and pattern recognition*, pages 770–778, 2016. 4
- [15] G. Hinton, O. Vinyals, and J. Dean. Distilling the knowledge in a neural network. In *NIPS workshop*, 2014. 2, 3
- [16] M. Hoai and F. De la Torre. Max-margin early event detectors. *International Journal of Computer Vision*, 107(2):191–202, 2014. 2
- [17] X. Jin, X. Li, H. Xiao, X. Shen, Z. Lin, J. Yang, Y. Chen, J. Dong, L. Liu, Z. Jie, et al. Video scene parsing with predictive feature learning. In *Computer Vision (ICCV), 2017 IEEE International Conference on*, pages 5581–5589. IEEE, 2017. 2
- [18] X. Jin, H. Xiao, X. Shen, J. Yang, Z. Lin, Y. Chen, Z. Jie, J. Feng, and S. Yan. Predicting scene parsing and motion dynamics in the future. In *Advances in Neural Information Processing Systems*, pages 6915–6924, 2017. 2
- [19] N. Kalchbrenner, A. v. d. Oord, K. Simonyan, I. Danihelka, O. Vinyals, A. Graves, and K. Kavukcuoglu. Video pixel networks. *arXiv preprint arXiv:1610.00527*, 2016. 1
- [20] K. M. Kitani, B. D. Ziebart, J. A. Bagnell, and M. Hebert. Activity forecasting. In *European Conference on Computer Vision*, pages 201–214. Springer, 2012. 2
- [21] A. Kundu, V. Vineet, and V. Koltun. Feature space optimization for semantic video segmentation. In *Proceedings of the IEEE Conference on Computer Vision and Pattern Recognition*, pages 3168–3175, 2016. 2
- [22] T. Lan, T.-C. Chen, and S. Savarese. A hierarchical representation for future action prediction. In *European Conference on Computer Vision*, pages 689–704. Springer, 2014. 2
- [23] J. Lezama, K. Alahari, J. Sivic, and I. Laptev. Track to the future: Spatio-temporal video segmentation with long-range motion cues. In *Computer Vision and Pattern Recognition (CVPR), 2011 IEEE Conference on*, pages 3369–3376. IEEE, 2011. 1, 2
- [24] Y. Li, H. Qi, J. Dai, X. Ji, and Y. Wei. Fully convolutional instance-aware semantic segmentation. In *2017 IEEE Conference on Computer Vision and Pattern Recognition (CVPR)*, pages 4438–4446. IEEE, 2017. 2
- [25] G. Lin, A. Milan, C. Shen, and I. D. Reid. Refinenet: Multi-path refinement networks for high-resolution semantic segmentation. In *CVPR*, volume 1, page 5, 2017. 1
- [26] T.-Y. Lin, P. Dollár, R. B. Girshick, K. He, B. Hariharan, and S. J. Belongie. Feature pyramid networks for object detection. In *CVPR*, volume 1, page 4, 2017. 1, 2, 3, 4
- [27] J. Long, E. Shelhamer, and T. Darrell. Fully convolutional networks for semantic segmentation. In *Proceedings of the IEEE conference on computer vision and pattern recognition*, pages 3431–3440, 2015. 1, 2, 3, 4
- [28] P. Luc, C. Couprie, Y. Lecun, and J. Verbeek. Predicting future instance segmentations by forecasting convolutional features. 2018. 1, 2, 5
- [29] P. Luc, N. Neverova, C. Couprie, J. Verbeek, and Y. Lecun. Predicting deeper into the future of semantic segmentation. In *IEEE International Conference on Computer Vision (ICCV)*, volume 1, 2017. 1, 2, 3, 5, 6

- [30] W. Luo, Y. Li, R. Urtasun, and R. Zemel. Understanding the effective receptive field in deep convolutional neural networks. In *Advances in neural information processing systems*, pages 4898–4906, 2016. 2
- [31] Z. Luo, J.-T. Hsieh, L. Jiang, J. C. Niebles, and L. Fei-Fei. Graph distillation for action detection with privileged information. In *European Conference on Computer Vision (ECCV)*, 2018. 3
- [32] B. Mahasseni, S. Todorovic, and A. Fern. Approximate policy iteration for budgeted semantic video segmentation. *arXiv preprint arXiv:1607.07770*, 2016. 2
- [33] J. Martinez, M. J. Black, and J. Romero. On human motion prediction using recurrent neural networks. In *2017 IEEE Conference on Computer Vision and Pattern Recognition (CVPR)*, pages 4674–4683. IEEE, 2017. 6
- [34] M. Mathieu, C. Couprie, and Y. LeCun. Deep multi-scale video prediction beyond mean square error. In *ICLR*, 2016. 1, 2
- [35] S. S. Nabavi, M. Roohan, and Y. Wang. Future semantic segmentation with convolutional lstm. In *BMVC*, 2018. 1, 2, 3, 4, 5, 6, 7, 8, 11, 12, 13
- [36] D. Nie, L. Wang, E. Adeli, C. Lao, W. Lin, and D. Shen. 3-d fully convolutional networks for multimodal isointense infant brain image segmentation. *IEEE Transactions on Cybernetics*, 2018. 4
- [37] Z. Qiu, T. Yao, and T. Mei. Learning spatio-temporal representation with pseudo-3d residual networks. In *ICCV*, 2017. 3
- [38] S. Ren, K. He, R. Girshick, and J. Sun. Faster r-cnn: Towards real-time object detection with region proposal networks. In *NIPS*, pages 91–99, 2015. 2
- [39] O. Ronneberger, P. Fischer, and T. Brox. U-net: Convolutional networks for biomedical image segmentation. In *International Conference on Medical image computing and computer-assisted intervention*, pages 234–241. Springer, 2015. 1, 2, 3, 4
- [40] L. Sevilla-Lara, D. Sun, V. Jampani, and M. J. Black. Optical flow with semantic segmentation and localized layers. In *Proceedings of the IEEE Conference on Computer Vision and Pattern Recognition*, pages 3889–3898, 2016. 2
- [41] K. Simonyan and A. Zisserman. Very deep convolutional networks for large-scale image recognition. *arXiv preprint arXiv:1409.1556*, 2014. 4
- [42] J. C. Stroud, D. A. Ross, C. Sun, J. Deng, and R. Sukthankar. D3d: Distilled 3d networks for video action recognition. *arXiv preprint arXiv:1812.08249*, 2018. 3
- [43] C. Vondrick, H. Pirsiavash, and A. Torralba. Anticipating visual representations from unlabeled video. In *Proceedings of the IEEE Conference on Computer Vision and Pattern Recognition*, pages 98–106, 2016. 1, 2
- [44] C. Vondrick, H. Pirsiavash, and A. Torralba. Generating videos with scene dynamics. In *Advances In Neural Information Processing Systems*, pages 613–621, 2016. 2
- [45] C. Vondrick and A. Torralba. Generating the future with adversarial transformers. In *IEEE Conference on Computer Vision and Pattern Recognition (CVPR)*, volume 1, page 3, 2017.
- [46] J. Walker, C. Doersch, A. Gupta, and M. Hebert. An uncertain future: Forecasting from static images using variational autoencoders. In *European Conference on Computer Vision*, pages 835–851. Springer, 2016. 2
- [47] S. Xingjian, Z. Chen, H. Wang, D.-Y. Yeung, W.-K. Wong, and W.-c. Woo. Convolutional lstm network: A machine learning approach for precipitation nowcasting. In *Advances in neural information processing systems*, pages 802–810, 2015. 4
- [48] S. Zagoruyko, A. Lerer, T.-Y. Lin, P. O. Pinheiro, S. Gross, S. Chintala, and P. Dollár. A multipath network for object detection. *arXiv preprint arXiv:1604.02135*, 2016. 2
- [49] K.-H. Zeng, W. B. Shen, D.-A. Huang, M. Sun, and J. C. Niebles. Visual forecasting by imitating dynamics in natural sequences. In *IEEE International Conference on Computer Vision (ICCV)*, volume 2, 2017. 1, 2
- [50] C. Zhang, L. Wang, and R. Yang. Semantic segmentation of urban scenes using dense depth maps. In *European Conference on Computer Vision*, pages 708–721. Springer, 2010. 2
- [51] H. Zhang, K. Dana, J. Shi, Z. Zhang, X. Wang, A. Tyagi, and A. Agrawal. Context encoding for semantic segmentation. In *The IEEE Conference on Computer Vision and Pattern Recognition (CVPR)*, 2018. 1
- [52] P. Zhang, J. Wang, A. Farhadi, M. Hebert, and D. Parikh. Predicting failures of vision systems. In *Proceedings of the IEEE Conference on Computer Vision and Pattern Recognition*, pages 3566–3573, 2014. 1
- [53] S. Zhou, D. Nie, E. Adeli, Y. Gao, L. Wang, J. Yin, and D. Shen. Fine-grained segmentation using hierarchical dilated neural networks. In *International Conference on Medical Image Computing and Computer-Assisted Intervention*, pages 488–496. Springer, 2018. 2

A. Supplementary Material

A.1. Analysis on Quantitative Result

In addition to quantitative comparisons with previous works, we analyze our forecasting results for each of the 19 classes of objects. Fig. 5 shows the IOU comparison for all classes over three different forecasting time-ranges, sorted in descending orders. One can notice that the prediction accuracy varies a lot across different classes. To better understand the reasons why certain classes have lower IOUs, we calculate the confusion matrix for all these classes, as shown in Fig. 6. The x-axis refers to the predicted class labels and the y-axis represents the ground-truth class labels. For instance, the ‘motorcycle’ class, which had the lowest results in Fig. 5 is mainly confused with the ‘bicycle’, ‘rider’, and ‘car’ classes. Additionally, we can vaguely see two light gray vertical lines for the ‘building’ and ‘vegetation’ predicted class labels. This shows that other classes are often mistaken with these two classes.

A.2. More Qualitative Results

Figs. 8, 9, 10 show more qualitative results for short-, mid-, and long-term forecasting, respectively. Each column represents one sample sequence, and the left-most two columns are the same samples from Fig. 3. Here, we also show the all input frames. From the inputs, we can easily observe the movements of different objects, such as pedestrians, cars, and bikes. We can also see that our predicted future semantic segmentation follows the observed motion patterns, and our results are closer to the ground-truth future semantic segmentation for all the three time-range settings. On the contrary, predicted segmentation boundaries by ConvLSTM [35] are not as smooth as ours. The two-stage method only works well for some examples in the

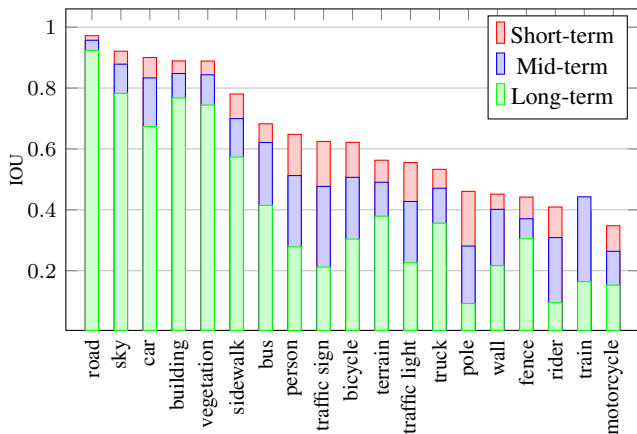


Figure 5. Per-class IOU for all 19 classes with respect to short, mid, and long-term forecasting. The forecasting performance varies a lot across different classes, implying that some classes are more difficult to correctly classify.

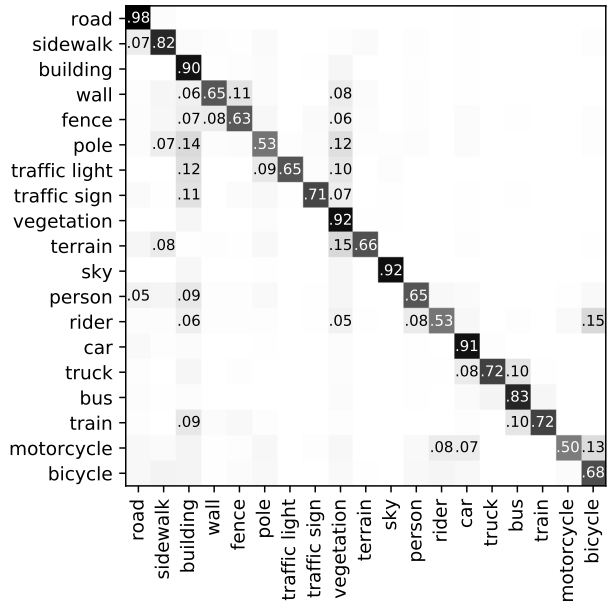


Figure 6. Confusion matrix of the mid-term semantic segmentation forecasting for all 19 classes in the Cityscapes dataset. The x-axis refers to the predicted class labels and the y-axis represents the ground-truth class labels. For instance, the confusion matrix shows that for some cases, the label ‘motorcycle’ is misclassified as ‘bicycle’, ‘rider’, and ‘car’.

short-term forecasting, and has difficulties in forecasting some mid- and long-term results.

A.3. Detailed Network Architecture

Fig. 7 shows the detailed architecture of our proposed network. The encoder module sequence can be seen in Table 4. The forecasting module is a temporal 3D convolution, and the decoder structure is symmetric to the encoder.

Table 4. Summary of one encoder pathway based on VGG19 backbone, applied to an input frame of size $H \times W$. Feature maps are defined as the output of the last convolution module in each block. Column ‘#’ denotes the number of repetitions of that module.

Module Sequence	#	Resolution	Channels
Input Frame		$H \times W$	3
3×3 Conv2D + BN + ReLU	2	$H \times W$	64
Max-Pool		$H/2 \times W/2$	64
3×3 Conv2D + BN + ReLU	2	$H/2 \times W/2$	128
Max-Pool		$H/4 \times W/4$	128
3×3 Conv2D + BN + ReLU	4	$H/4 \times W/4$	256
Max-Pool		$H/8 \times W/8$	256
3×3 Conv2D + BN + ReLU	4	$H/8 \times W/8$	512
Max-Pool		$H/16 \times W/16$	512
3×3 Conv2D + BN + ReLU	4	$H/16 \times W/16$	512

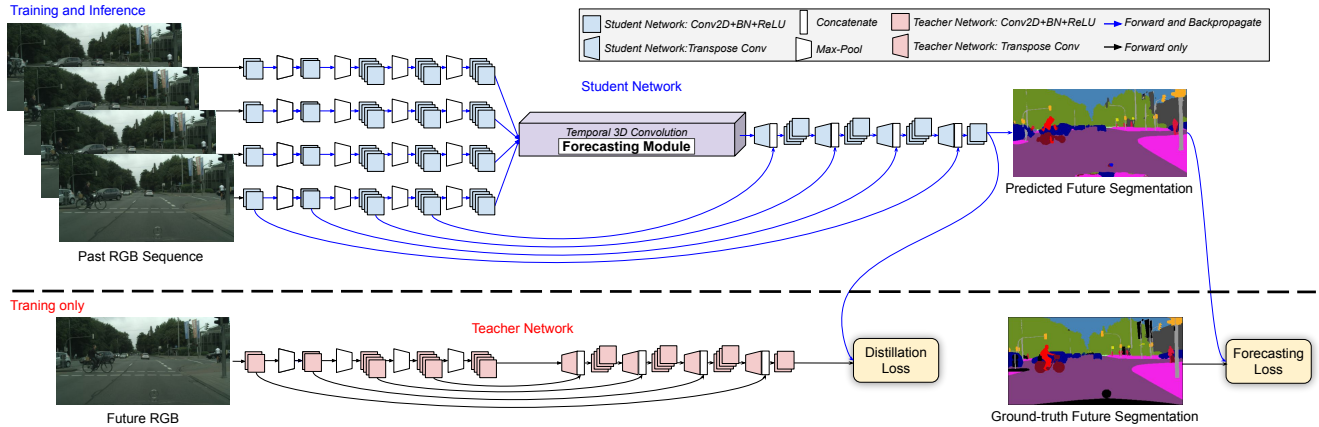


Figure 7. Network architecture overview: our student network contains encoder, forecasting module, and decoder. The encoder takes the past frames and learns latent low-dimensional representations by gradually decreasing the resolution. Our forecasting module then merges them by a temporal 3D convolution that maps them to the future. Finally, the decoder gradually increases the resolution of the output segmentation while having skip connections with the encoder at each resolution. The stacked instances of blue blocks are convolutional modules connected in a sequence. The teacher network has the same encoder and decoder architecture as the student network, but without sharing trainable parameters.

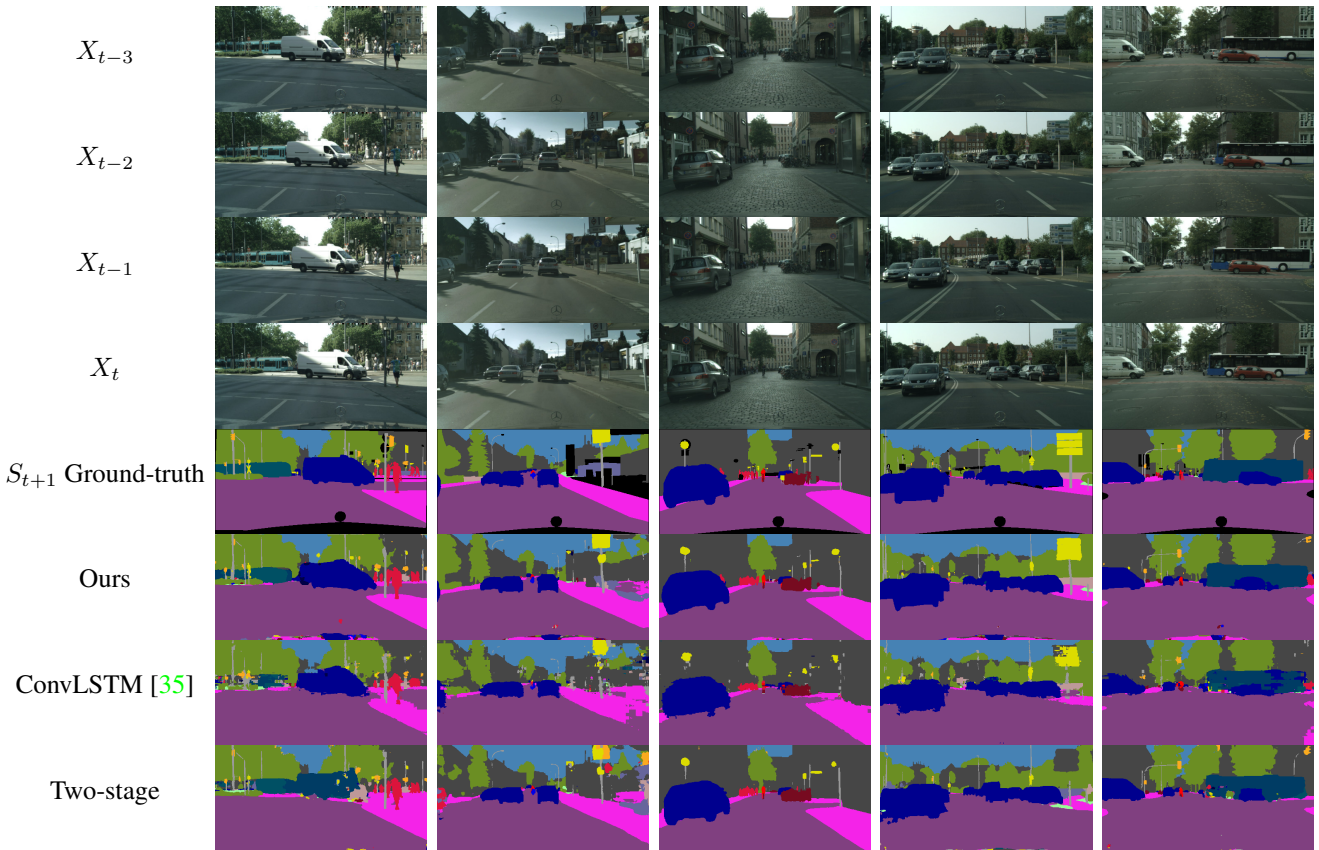


Figure 8. More short-term forecasting qualitative results.

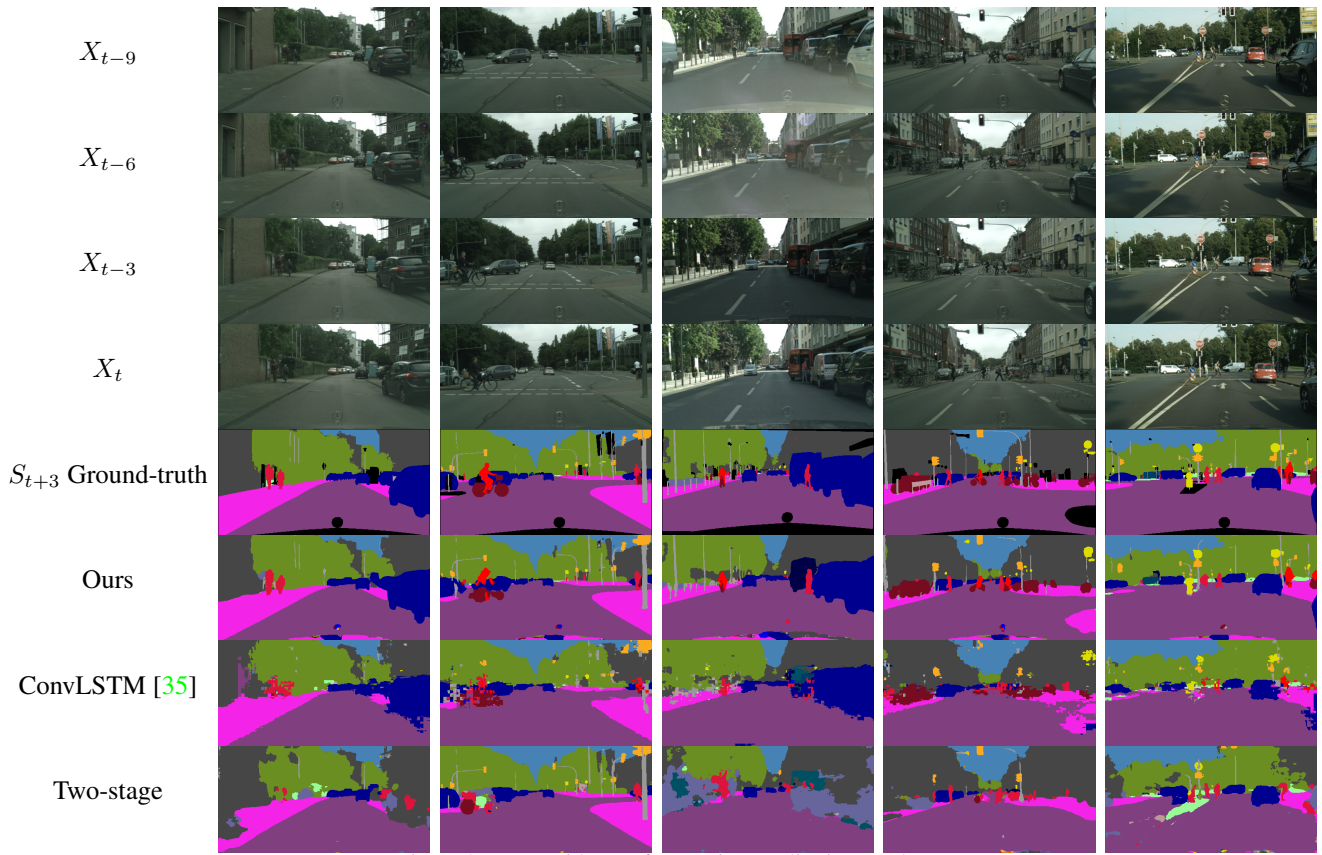


Figure 9. More mid-term forecasting qualitative results.

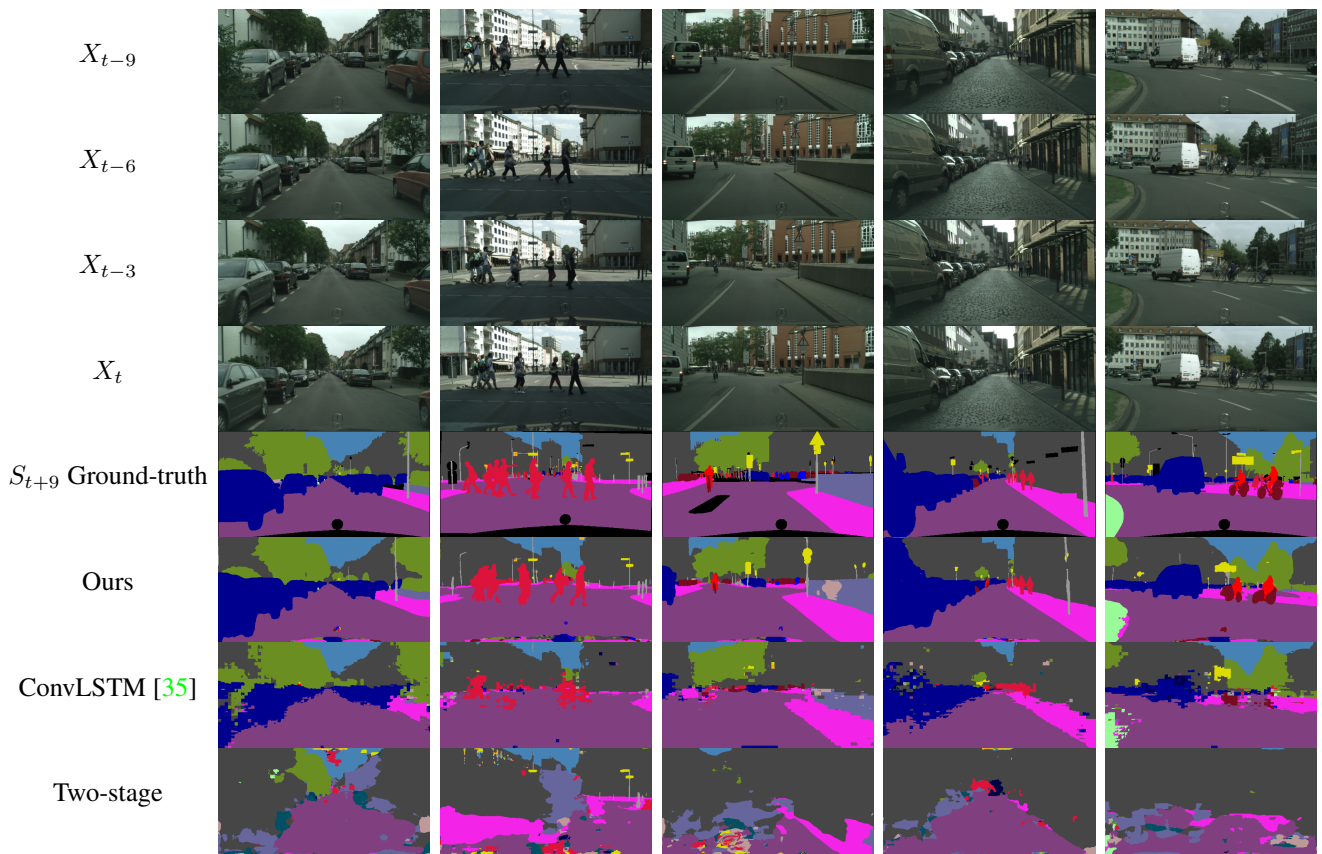


Figure 10. More long-term forecasting qualitative results.